Chapter 6: Microdischarge Synthesis of Fe Nanoparticles for Diameter-Controlled Growth of Carbon Nanotubes

6.1. Introduction

Nanometer-sized materials represent the future building blocks of nanoscale structures and often exhibit novel properties. These novel properties often are size dependent due to quantum effects. In particular, these properties have been increasing explored for carbon nanotubes (CNTs).[*1-3*] Tseng and co-workers have shown that the CNT diameter affects the on- and off-state currents in CNT transistors.[*4*] Theoretically, Kutana and Giapis demonstrated that the mechanical properties of CNTs are size dependent.[*5*] Accordingly, several studies have focused on the synthesis of CNTs with a narrow size distribution.[*6-10*]

Dai and co-workers reported CNT growth by chemical vapor deposition (CVD) from iron oxide nanoparticles derived from artificial ferritin.[*9*] Discrete iron oxide nanoparticles with an average diameter of 1.9 and 3.7 nm were obtained by placing a different number of iron atoms into the core of apoferritin. These particles were utilized subsequently to grow CNTs with mean diameters of 1.5 nd 3.0 nm, respectively. Beyond establishing a correlation between particle and nanotube size, the size dispersity of the nanoparticle and nanotube were found to be similar as well. This correspondence between nanoparticle and nanotube size dispersity was confirmed using polyaminoamine dendrimers to limit the nanoparticle size dispersity. As hypothesized, the narrower

particle size distribution resulted in tighter control over the CNT diameter distribution.[*7*] Beyond this limited range, the size correlation between CNT and nanoparticle diameter was extended to the synthesis of CNTs in the range of 3 to 13 nm.[*6*]

In these studies, the nanotube diameter was measured with either AFM or TEM to be smaller than the average nanoparticle diameter from which they grow. While the correlation provides a practical criterion for controlling the nanotube size, the actual nanoparticle size before and during nanotube growth could be quite different. In a typical CNT growth, a strongly reducing environment is used and should reduce the oxidized nanoparticle size since above a temperature of 750 K, Fe_2O_3 is reduced to Fe in the presence of hydrogen.[*11*] While measuring the metal nanoparticle size without oxidation is difficult using AFM and TEM, we present preoxidation size measurements of iron nanoparticles produced in an atmospheric-pressure microdischarge. To provide a size correlation between the nanoparticle and the CNT, we further show the resulting nanotube diameter distribution and the nanoparticle size after growth.

6.2. Experimental Method

The iron nanoparticle synthesis strategy originates from a previous report[*12*] in which silicon nanoparticles with an average diameter of 1.6 nm were synthesized using a hollow cathode microdischarge. Exchanging the argon stream containing the silane precursor with an ultra-high purity (UHP) argon stream that flows over ferrocene powder allowed the same experimental setup to be used to generate Fe nanoparticles, as depicted in figure 6.1. Ferrocene powder (>98% pure) was used as the Fe source since it sublimes at room temperature with a vapor pressure of 12 mTorr.[*13*] This vapor pressure is high enough to generate nanoparticles in the microdischarge yet sufficiently low to do so

without clogging the micro-hollow cathode (I. D. ≈ 180 μm). The ferrocene concentration was controlled via dilution of the ferrocene-saturated UHP argon stream with a second UHP argon stream. The relative flow rates of these two streams were adjusted to vary the ferrocene concentration in the gas mixture, while maintaining a combined flow rate of 150 standard cubic centimeters per minute (sccm). All ferrocene concentrations were calculated assuming that the gas stream flowing over the ferrocene was saturated.

This gas mixture was passed through a stainless steel capillary tube that served as the cathode of a direct current microdischarge. The discharge formed inside of the stainless steel capillary tube with an afterglow extending to a second grounded metal tube (anode, I. D. ≈ 2 mm). The electrodes were separated by a gap of 1.5 mm and were sealed inside a quartz tube using UltraTorr fittings (0.5 inch). A sheath flow of Ar was combined with the particle stream in the afterglow region of the microdischarge to prevent particle coagulation and to limit particle loss to the walls. The typical voltage and current used to sustain the discharge were −180 V and 7.5 mA, respectively. The microdischarge was operated at a pressure slightly above atmospheric averting the need for vacuum pumps. The spatially confined microdischarge served as a short residence time reactor, where the sublimed precursor was decomposed by electron impact collisions and rapid gas heating. Particle nucleation and growth in the discharge is believed to be abruptly terminated once the particles are swept out of the discharge region by the flow.

The continuous stream of Fe nanoparticles thus produced was monitored *in situ* for particle size distribution using a newly developed radial differential mobility analyzer (nano-RDMA), which was calibrated using electrospray of quaternary amines.[*14*] The

nano-RDMA was operated in stepping mode using a 10 standard liters per minute sheath flow, which were the same conditions used to calibrate the instrument.

Alternative to size measurement, nanoparticles were collected thermophoretically in a stagnation-point-flow geometry over a cleaned Si wafer (8 mm x 8 mm with 500 nm thermal SiO_2) for both *ex situ* particle sizing and nanotube growth. The thermophoretic collector consisted of a round upper plate heated to ~200^{o}C and a lower substrate holder, cooled using a mixture of dry ice and acetone. Although some of the particles were charged and electrostatic collection was possible, thermophoretic deposition was chosen over electrostatic precipitation so that the fraction collected was not influenced by the charge distribution on the aerosol. Once collected, the substrates were stored under nitrogen in a dessicator until commencing CNT growth to limit oxidation and water absorption.

The nanoparticle-decorated Si substrates were used to grow CNTs through a chemical vapor deposition (CVD), as described previously.[*15*] The substrates were placed in a tube furnace and heated to 900^{o}C while under a flow of argon (500 sccm) and allowed to equilibrate at the elevated temperature for 10 minutes. Hydrogen (100 sccm) was added to the argon flow for 10 minutes to reduce the nanoparticles that have oxidized. Subsequently, methane was added at 1000 sccm to the other two flows for 7 minutes to generate CNTs. To ensure few defects, the hydrogen and argon flow were continued for another 10 minutes. Finally, the furnace was cooled down under an argon flow to room temperature to prevent oxidative degradation of the nanotubes.

These substrates were imaged with an atomic force microscope (AFM) (Digital Instruments with a Nanoscope IV controller) before and after carbon nanotube growth. Multiple images (2 μm x 2 μm in size) of the wafers were captured in tapping mode to permit statistical analysis of the carbon nanotube diameters. As the width of features represents a convolution of the tip and the actual nanoparticle size, the measured height above the substrate was recorded as the diameter of the nanotube or particle.

6.3. Results and Discussion

The Fe nanoparticle size distributions measured with the nano-RDMA indicated that mean particle size and the breadth of the distribution increased with the ferrocene concentration, as shown in figure 6.2. Since these measurements are made *in situ*, these diameters pertain to the unoxidized nanoparticle. Fitting the obtained distributions to a log-normal function provided the geometric mean particle diameter (D_g) and standard geometric deviation (σ_g).

For the lower concentrations investigated, the particle size was narrowly distributed (σ_g <1.2), as desired for tight control over the resulting nanotube diameters. Above 5 ppm, the large σ_g values (σ_g >1.3) were indicative of particle agglomeration, which causes the measured particle size to appear larger than their actual size. Based on these values, it appears that the limited residence time of the microdischarge hindered nanoparticle growth beyond 3.5 nm. While increasing the cathode diameter would increase the residence time, the intense microdischarge would not fill the entire volume of the larger cathode,[*16*] resulting in a residence time distribution that would not be appropriate for correlating nanoparticle size to nanotube diameter.

The nano-RDMA data also demonstrated that the particle number density increased with ferrocene concentration. Accordingly, different nanoparticle densities were observed in the AFM images of the wafers after five minutes of thermophoretic deposition. While increasing the deposition time correspondingly increased the nanoparticle density, sparse nanoparticle coverage was desired to limit surface diffusion of particles, to avoid particle sintering during nanotube growth, and to ensure minimal overlap between nanotubes. In addition to observing nanoparticle density variation, the AFM images corroborated the size measured using the nano-RDMA, with the AFM measured average size appearing slightly larger than the nano-RDMA size likely due to environmental oxidation.

Using the nanoparticle coated samples, nanotubes were grown as the representative images in figure 6.3A,B demonstrate, where the ferrocene concentration used for nanoparticle synthesis was 1 and 5 ppm, respectively. The nanotubes shown in figure 6.3B exhibit more color contrast (i.e., topographical height variation) compared to those in figure 6.3A, which indicates that the diameters of the nanotubes are larger for the larger nanoparticles. Additionally, the inset in figure 6.3A appears to depict a nanoparticle at the end of the nanotube, confirming the catalytic nature of the particle.

To obtain statistical information, height measurements of more than 100 individual CNTs were made for each concentration. The distribution of nanotube heights for five different ferrocene concentrations are shown in figure 6.4 with the corresponding size distribution parameters listed in table 6.1. The average CNT diameter increases with the ferrocene concentration from 1 to 5 ppm with standard deviations around 0.77 to 0.85 (values comparable to other reports).[*17-20*] The average CNT

diameter was found to be larger than the Fe nanoparticle diameter measured using the nano-RDMA. While this correlation is different than previous reports, it has been observed when monitoring nanotube growth *in situ* in an Environmental TEM from a nickel nanoparticle that has been reduced.[*21*]

Beyond measuring the nanotube size, the nanoparticle size after carbon nanotube growth was recorded as well for particles growing CNTs as well as those that did not catalyze CNT growth for comparison. A compilation of all the size data is shown in figure 6.5 as a function of ferrocene concentration. The size of nanoparticles growing CNTs also increased with ferrocene concentration, but did not remain proportionally larger than the CNT diameter. It is important to note that despite collecting numerous images for the 1 ppm concentration, very few ends of the CNTs were observed in the AFM images and therefore an average size is not presented.

A more interesting trend is observed for those nanoparticles not catalyzing CNT growth. For low ferrocene concentrations (i.e., small nanoparticle size), the nanoparticles not growing CNTs are the same size as those that did. This indicates all nanoparticles experience a similar growth environment and that the methane supply is sufficient to decompose and enlarge all of the particles uniformly. For particles produced with high ferrocene concentrations (i.e., large nanoparticle size), the nanoparticle sizes after growth are more similar to the size of the pre-growth nanoparticle. The observed difference in average size is due to a few particles much larger than the average size. This indicates that methane primarily goes toward CNT growth once CNTs have nucleated on the larger nanoparticles. Also, it confirms that the CNT growth conditions do not result in particle sintering, but rather that a different mechanism is responsible for the observed size

increase. The most obvious route leading to the observed size increase would be the catalytic decomposition of methane on the nanoparticle surface and carbon uptake in the nanoparticle.[*22*]

While the nanoparticle size after CNT growth is not consistently proportional to the CNT diameter, a clear correlation between the CNT size and the pre-growth nanoparticle size is observed with the CNT size larger by a factor of two over the nano-RDMA measured size. We believe the difference in size between the CNT diameter and the pre-growth nanoparticle size can be explained through examining the growth mechanism. It appears that the reduced Fe nanoparticle initially enlarges due to carbon uptake.[*22*] After reaching carbon saturation, a nanotube nucleates from the surface.[*23*] The overall result is a nanotube that is larger than the initial Fe nanoparticle.

6.4. Summary

The use of a microdischarge for the synthesis of Fe nanoparticles with a very narrow size distribution has been demonstrated. Using these particles, we have catalytically grown CNTs and shown that these CNTs have a diameter larger than the unoxidized particle diameter through comparing AFM and nano-RDMA measurements. After CNT growth, we have shown that the particles growing nanotubes appear larger than the CNT diameter. Examining these size distributions, we have shown that the pre-growth particle size shows a clearer correspondence to the CNT average diameter than does the post-growth nanoparticle size.

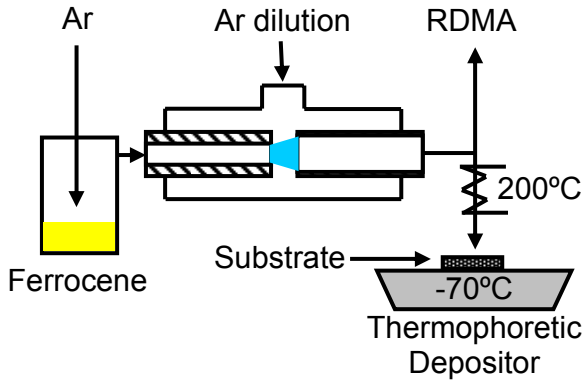

Figure 6.1 Schematic of Microplasma for Fe Nanoparticles.

Schematic of the microplasma and thermophoretic depositor used for Fe nanoparticle synthesis and collection. The heating was achieved with a feedback controlled heat rope whereas the cooling was achieved with a dry ice and acetone bath.

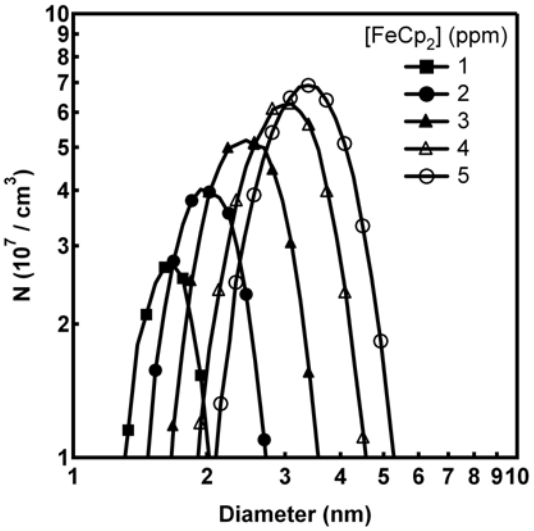

Figure 6.2. Size Distributions of Iron Nanoparticles.

Size distributions of Fe nanoparticles measured *in situ* using a nano-RDMA.

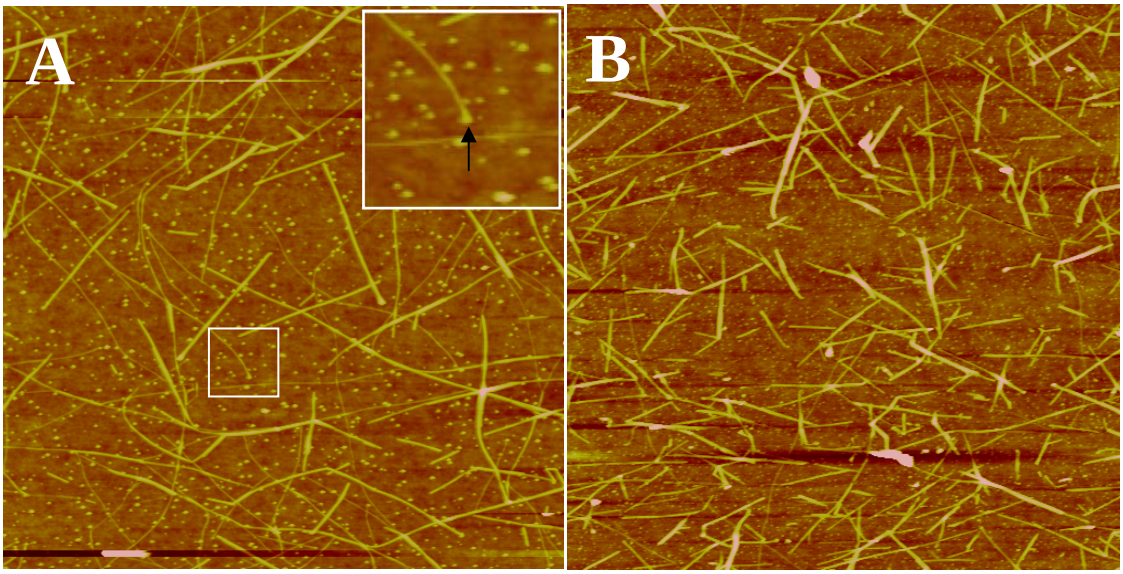

Figure 6.3. AFM Images of CNTs.

2 μm × 2 μm AFM images with ferrocene concentrations of (A) 2 ppm and (B) 5 ppm. The inset of **3A** is a 300 nm × 300 nm magnified image.

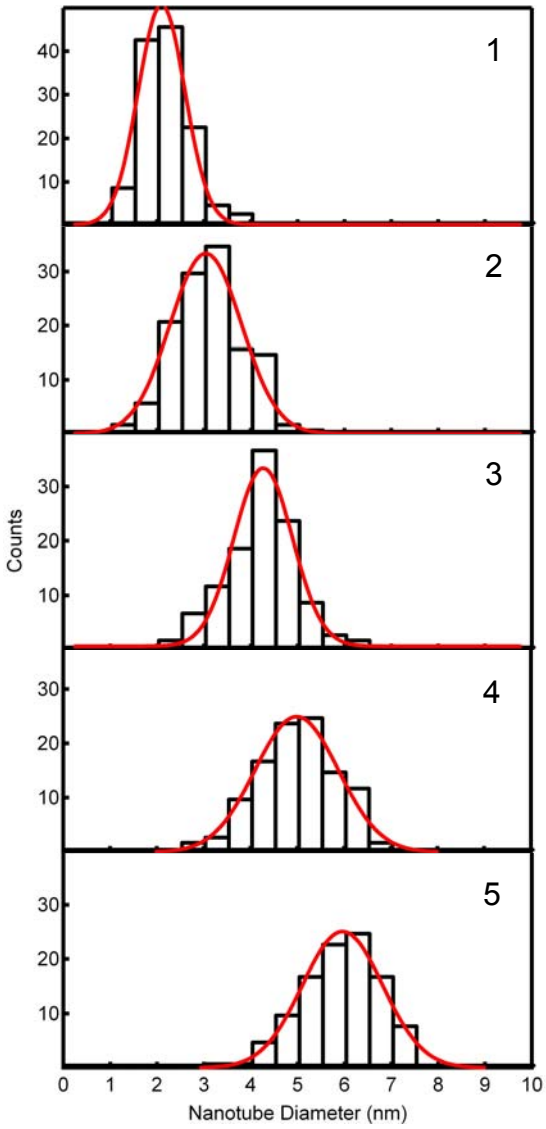

Figure 6.4. Size Distribution of Nanotube Diameters.

Diameter distribution of CNTs obtained from AFM height measurement. The Fe nanoparticles were produced from Ar/ferrocene stream at the indicated ferrocene concentrations in parts per million (ppm).

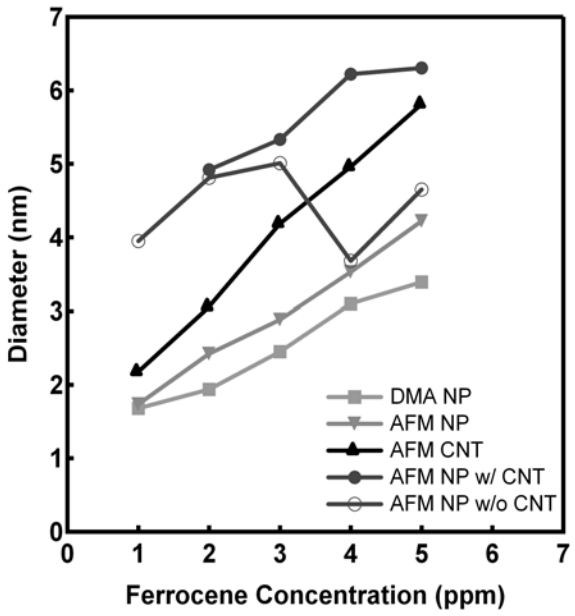

Figure 6.5. Size Variation of Nanotubes and Nanoparticles.

Effect of ferrocene concentration in the Ar/ferrocene stream used to synthesize Fe nanoparticles on the average nanoparticle size before (nano-RDMA and AFM) and after CNT growth. The average CNT diameter measured with AFM is included for reference.

Table 6.1 Measured Particle Size.

Average particle size measured before (with the nano-RDMA and AFM) and after CNT growth (with AFM). The average nanotube diameter is included for reference.

	Before		After		
[Ferrocene] (ppm)	nano-RDMA NP Size (nm)	AFM NP Size (nm)	AFM CNT Size (nm)	AFM NP Size w/ CNT (nm)	AFM NP Size w/o CNT (nm)
1	1.08	1.74	2.18	-	3.95
2	1.34	2.42	3.06	4.92	4.81
3	1.85	2.89	4.19	5.33	5.01
4	2.50	3.53	4.96	6.22	3.68
5	2.79	4.22	5.82	6.30	4.85

References

1. V. N. Popov, *Mat Sci Eng R,* **43**, 61, Jan 15, 2004.
2. C. N. R. Rao, B. C. Satishkumar, A. Govindaraj, and M. Nath, *Chemphyschem,* **2**, 78, Feb 16, 2001.
3. M. Terrones, *Int Mater Rev,* **49**, 325, Dec, 2004.
4. Y. C. Tseng, K. Phoa, D. Carlton, and J. Bokor, *Nano Lett,* **6**, 1364, 2006.
5. A. Kutana, and K. P. Giapis, *Physical Review Letters,* **97**, 245501, 2006.
6. C. L. Cheung, A. Kurtz, H. Park, and C. M. Lieber, *J. Phys. Chem. B,* **106**, 2429, 2002.
7. H. C. Choi, W. Kim, D. Wang, and H. Dai, *The Journal of Physical Chemistry B,* **106**, 12361, 2002.
8. S. Han, T. Yu, J. Park, B. Koo, J. Joo, T. Hyeon, S. Hong, and J. Im, *Journal of Physical Chemistry B,* **108**, 8091, 2004.
9. Y. Li, W. Kim, Y. Zhang, M. Rolandi, D. Wang, and H. Dai, *Journal of Physical Chemistry B,* **105**, 11424, 2001.
10. Q. Fu, S. Huang, and J. Liu, *J. Phys. Chem. B,* **108**, 6124, 2004.
11. O. J. Wimmers, P. Arnoldy, and J. A. Moulijn, *The Journal of Physical Chemistry,* **90**, 1331, 1986.
12. R. M. Sankaran, D. Holunga, R. C. Flagan, and K. P. Giapis, *Nano Lett,* **5**, 531, 2005.
13. L. A. Torres-Gomez, G. Barriero-Rodriguez, and F. Mendez-Ruiz, *Thermochimica Acta,* **124**, 179, 1988.

14. N. A. Brunelli, R. C. Flagan, and K. P. Giapis, *Submitted to Aerosol Science and Technology.*, 2008.

15. L. A. Wade, I. R. Shapiro, Z. Y. Ma, S. R. Quake, and C. P. Collier, *Nano Lett.,* **4**, 725, Apr, 2004.

16. R. M. Sankaran, *Journal of Applied Physics,* **92**, 2406, 2002.

17. H. C. Choi, W. Kim, D. W. Wang, and H. J. Dai, *J. Phys. Chem. B,* **106**, 12361, Dec, 2002.

18. C. L. Cheung, A. Kurtz, H. Park, and C. M. Lieber, *J. Phys. Chem. B,* **106**, 2429, Mar, 2002.

19. Y. M. Li, W. Kim, Y. G. Zhang, M. Rolandi, D. W. Wang, and H. J. Dai, *J. Phys. Chem. B,* **105**, 11424, Nov 22, 2001.

20. Q. Fu, S. M. Huang, and J. Liu, *J. Phys. Chem. B,* **108**, 6124, May, 2004.

21. R. Sharma, P. Rez, M. M. J. Treacy, and S. J. Stuart, *Journal of Electron Microscopy,* **54**, 231, 2005.

22. A. R. Harutyunyan, T. Tokune, E. Mora, J. W. Yoo, and A. J. Epstein, *Journal of Applied Physics,* **100**, 044321, 2006.

23. W. H. Chiang, and R. M. Sankaran, *Applied Physics Letters,* **91**, 121503, 2007.